SIAM J. APPL. MATH.
Vol. 59, No. 4, pp. 1335–1355

CHAIN-BRANCHING EXPLOSIONS IN MIXING LAYERS*

ANTONIO L. SÁNCHEZ†, AMABLE LIÑÁN‡, AND FORMAN A. WILLIAMS§

Abstract. The chain-branching process leading to ignition in the high-temperature hydrogen-oxygen mixing layer is studied by application of a novel WKB-like method when, as is typically the case, two branching radicals cannot be assumed to maintain steady state. It is shown that the initiation reactions, responsible for the early radical buildup, cease being important when the radical mass fractions reach values of the order of the ratio of the characteristic branching time to the characteristic initiation time, a very small quantity at temperatures of practical interest. The autocatalytic character of the chain-branching reactions causes the radical concentrations to grow exponentially with downstream distance in the process that follows. It is shown that the transverse radical profiles that emerge can be described by exponential series of the WKB type in inverse powers of the streamwise coordinate. The analysis reveals that, because of the effect of radical diffusion, the rate of radical growth is uniform across the mixing layer in the first approximation, with the exponential growth in distance having the same nondimensional streamwise variation as that of a premixed branching explosion evaluated at the transverse location where the effective Damköher number based on the flow velocity and branching rate is maximum. This functional streamwise variation, as well as the leading-order representation of the radical profiles, is obtained by imposing a condition of bounded, nonoscillatory behavior on the solution. The resulting radical profiles peak at the location of maximum local Damköhler number and decay exponentially to the sides. Analysis of the solution in the vicinity of the maximum, which is a turning point of second order in the WKB expansion, yields the second-order correction to the growth rate as an eigenvalue in a linear eigenvalue problem. The method developed can be extended to the analysis of chain-branching explosions in laminar, self-similar mixing layers with an arbitrary number of branching steps adopted for describing the chemistry.

Key words. WKB, chain branching, mixing layers

AMS subject classifications. 76V05, 76D30

PII. S003613999732648X

1. Introduction.

The processes leading to autoignition in nonpremixed mixing layers have been widely studied in recent years. Both coflow and counterflow configurations with the boundary-layer approximation adopted for the conservation equations have been considered, yielding problems that are, respectively, parabolic and elliptic [5, 6]. Depending on the underlying chemistry, two different explosion behaviors can be identified: thermal ignition and chain-branching ignition. The former, which is characterized by abrupt temperature increases, can be investigated with a one-step Arrhenius model adopted for the chemistry, whereas chain-branching processes, in which the radical pool increases, can be isothermal, but typically require a number of chemistry steps for their description.

The study of nonpremixed spontaneous ignition in the coflow mixing layer, with

*Received by the editors August 27, 1997; accepted for publication (in revised form) June 18, 1998; published electronically April 27, 1999.
http://www.siam.org/journals/siap/59-4/32648.html

†Escuela Politécnica Superior, Universidad Carlos III de Madrid, Butarque 15, 28911 Leganés, Spain (asanchez@ing.uc3m.es). The research of this author was supported by the Spanish DGICYT under contract PB95-0296.

‡E. T. S. I. Aeronáuticos, Universidad Politécnica de Madrid, Cardenal Cisneros 3, 28040 Madrid, Spain. The research of this author was supported by the Spanish CICYT under contract PB94-0400 and by INTA under contract INTA 4070-0036/1995.

§Center for Energy and Combustion Research, University of California San Diego, La Jolla, CA 92093-0411 (faw@karman.ucsd.edu). The research of this author was supported by the National Science Foundation under grant NSF ACTS 95-26410.

a one-step Arrhenius model adopted for the chemistry, was performed by Liñán and Crespo [6], who took advantage of the large value of the activation energy typical of combustion processes for their asymptotic analysis. They found that the evolution of reactive mixing layers is characterized by an initial quasi-frozen stage in which the two streams mix and begin to react, followed by a sudden explosion or thermal runaway that clearly identifies the ignition location. An extension of the thermal-runaway analysis of Liñán and Crespo [6] to take into account the wake that forms downstream from the splitter plate initially separating the streams has recently been published [9].

Analytical studies of chain-branching explosions in both the counterflow and the coflow mixing layers have been conducted in recent years for hydrogen-air systems with free-stream temperatures above the crossover temperature at which the rate of the main chain-terminating reaction $H + O_2 + M \rightarrow HO_2 + M$ equals that of the rate-controlling branching reaction $H + O_2 \rightarrow OH + O$ [13]. In particular, it has been shown that the ellipticity associated with the counterflow configuration causes the branch of ignited solutions to emerge as a bifurcation from the frozen state [7, 8]. In contrast, chain-branching ignition in coflow mixing layers is a parabolic problem that leads to a continuous growth of the radical pool in a self-accelerating manner [10, 14]. If the temperature is sufficiently above crossover, then the effect of three-body recombination reactions, responsible for most of the heat released in H_2-O_2 combustion, is negligible, and the two streams mix and react initially without significant chemical heating. This gives rise to a thermally frozen branched-chain explosion [10]. In the early stages of the process, radical concentrations are very small, and the slow initiation steps control the process. Very soon the radical pool becomes large enough for the branching steps to take over, giving rise downstream to exponentially increasing radical concentrations. This region of autocatalytic growth, which is much longer than the initial initiation-controlled region, ends where the mass fractions of the radicals achieve their peak mole fractions, of order unity, corresponding to partial equilibrium of the branching reactions. Downstream from this ignition point there is a region of radical recombination with significant heat release which leads to the development of a diffusion flame, a process addressed elsewhere [11].

Following our previous work [10], we study here the isothermal radical-growth process leading to ignition in the hydrogen-air coflow mixing layer for temperatures above crossover with a chemistry description that includes two branching radicals not in steady state. Asymptotic solutions for both the initiation-controlled region and the region of autocatalytic growth will be obtained by considering the limits of small and large values of the normalized streamwise distance, respectively. Analysis of the region of autocatalytic growth, which determines in the first approximation the location of the ignition point and the shape of the associated radical profiles, will be developed by utilizing WKB-like exponential expansions for the radical concentrations in a series of decaying powers of the streamwise distance, extending the analysis to obtain the second-order correction to the ignition distance. Use of two branching radicals, which was done only at leading order in our previous work [10], is needed for accurate descriptions of real systems [2, 8]. It may thus be worth emphasizing that previous numerical and analytical studies [2, 8, 10] have demonstrated clearly that physically correct and accurate analytical representations of the real chemistry and ignition process in hydrogen-air evolving mixing layers under the high-temperature conditions addressed here require a treatment of the present type.

The problem is formulated in the next section. The characteristic scales associ-

ated with the igniting mixing layer as well as the character of the resulting solution are next anticipated in section 3. In section 4 we develop the asymptotic solution. Discussion of the results, including comparisons of the asymptotic predictions with results of numerical integrations of the conservation equations, is presented in section 5. Finally, conclusions are given in section 6.

2. Formulation. If the temperature of the coflowing streams is sufficiently above crossover, as is the case considered in the present study, then the effect of three-body recombination reactions is negligible, and the initiation reaction

$$H_2 + O_2 \xrightarrow{1} OH + OH$$

and radical-branching reactions

$$H + O_2 \xrightarrow{2} OH + O,$$

$$H_2 + O \xrightarrow{3} OH + H,$$

and

$$H_2 + OH \xrightarrow{4} H_2O + H$$

suffice to describe the branched-chain process of hydrogen-oxygen chemistry. Although reaction 1 is slow because of its large activation energy, it must be retained in the mechanism to provide the first radicals when upstream diffusion is negligible, as is the case in the present study. In the ignition region the characteristic mass fractions of radicals and that of water vapor are small quantities. This causes the rates of the reverse reactions 2–4, proportional to products of small mass fractions, to be negligible compared with the forward rates retained in the analysis, which are linearly proportional to radical mass fractions. This holds during the radical growth process until the radical mole fractions increase to values of order unity such that the rates of the backward reactions 2–4 become comparable to those of the branching steps, ushering in a thin region across which the branching reactions reach partial equilibrium. Because of the rapid radical growth that will be seen to characterize the process, the backward reactions 2–4 are significant only very close to the ignition point, and they are consequently neglected in the analysis that follows.

The chemical scheme 1–4 can be further simplified by assuming that the OH radical maintains steady state everywhere, an assumption motivated by the relatively large rate of reaction 4 that has been numerically tested in a previous study [2]. The OH radicals produced by reactions 1–3 are then readily consumed by reaction 4 before they can be transported, so that, for instance, the overall effect of reaction 1, which produces two OH radicals, can be obtained by twice adding reaction 4 to reaction 1 to give the global initiation reaction

$$3H_2 + O_2 \xrightarrow{\text{I}} 2H + 2H_2O,$$

with a rate given by that of the elementary reaction 1. Similarly, by adding reactions 2 and 4 and reactions 3 and 4, one can easily derive the global branching reactions

$$H_2 + O_2 \xrightarrow{\text{II}} O + H_2O$$

and

$$2H_2 + O \xrightarrow{\text{III}} 2H + H_2O,$$

with rates given, respectively, by those of the elementary reactions 2 and 3. The reaction-rate constants corresponding to the elementary steps 1–3 are of the form $k_j = A_j T^{n_j} \exp[-E_j/(R^o T)]$, where R^o is the universal gas constant. Updated values of the different reaction-rate parameters in mol/cm^3, s^{-1}, K, and cal/mol are [3] $A_1 = 1.7 \times 10^{13}$, $A_2 = 3.52 \times 10^{16}$, $A_3 = 5.06 \times 10^4$, $n_1 = 0$, $n_2 = -0.7$, $n_3 = 2.67$, $E_1 = 47780$, $E_2 = 17070$, and $E_3 = 6290$.

We consider a laminar mixing layer consisting of two parallel streams, one of hydrogen diluted with nitrogen and the other of air. In the formulation, x and y will be the coordinates in the streamwise and transverse directions, with u and v being their corresponding velocity components. The air and fuel streams occupy initially the upper ($y > 0$) and lower ($y < 0$) sides, merging at $x = 0$ where mixing and reaction begin. The subscripts ∞ and $-\infty$ will denote, respectively, free-stream conditions on the air and fuel sides. We shall assume that density ρ and transport properties are constant, a simplifying assumption that may introduce some degree of inaccuracy in the calculation when the temperatures of the merging streams are different, and also for undilute fuel feed as shown in [8]. For the flow considered, there exist self-similar solutions for the velocity field, the frozen reactant concentrations, and the frozen temperature distribution, which are obtained by use of a similarity coordinate $\eta = [u_\infty/\nu]^{1/2} y/x^{1/2}$ and a nondimensional stream function $F(\eta)$, such that $u = u_\infty F'$ and $v = (\nu u_\infty/x)^{1/2}(\eta F' - F)/2$, where the prime denotes differentiation with respect to η and ν is the kinematic viscosity of the mixture [15]. With these new variables, the boundary-layer equations for the thermally frozen mixing layer with N different reactive species become

$$\frac{1}{2} F F'' + F''' = 0, \tag{2.1}$$

$$F' \frac{\partial Y_i}{\partial x} - \frac{1}{x}\left(\frac{1}{2} F Y_i' + \frac{1}{S_i} Y_i''\right) = \frac{w_i}{\rho u_\infty}, \tag{2.2}$$

and

$$\frac{1}{2} F \theta' + \frac{1}{Pr} \theta'' = 0, \tag{2.3}$$

where $\theta = (T - T_\infty)/T_\infty$ is an appropriate nondimensional temperature defined with respect to the air-side temperature, $Pr = \mu c_p/\lambda$ is the Prandtl number, with c_p being the specific heat at constant pressure of the mixture, and Y_i, $S_i = \mu/(\rho D_i)$ and w_i are, respectively, the mass fraction, Schmidt number, and mass rate of production of species i. The transport coefficients λ and D_i correspond to the thermal conductivity of the mixture and the binary diffusion coefficient of species i. Equations (2.1)–(2.3) must be integrated subject to the boundary conditions $F' = 1$, $Y_i = Y_{i\infty}$, and $\theta = 0$ at $\eta = \infty$; $F' = u_{-\infty}/u_\infty$, $Y_i = Y_{i-\infty}$, and $\theta = \theta_{-\infty} = (T_{-\infty} - T_\infty)/T_\infty$ at $\eta = -\infty$; and $F = 0$ at $\eta = 0$. In addition to the above boundary conditions, one must provide initial conditions for the integration of (2.2) given by the uniform free-stream profiles $Y_i = Y_{i\infty}$ for $\eta > 0$ and $Y_i = Y_{i-\infty}$ for $\eta < 0$.

With the simplifying assumptions introduced, (2.1) is decoupled and can be integrated separately to yield the self-similar solution for the velocity profile, whereas the self-similar frozen solutions for the temperature and reactant profiles can be determined by integration of (2.3) together with the frozen version of (2.2) with the

previously stated boundary conditions to yield

$$y_{O_2 f} = \frac{\int_{-\infty}^{\eta} \exp\left[-(S_{O_2}/2)\int_0^{\bar{\eta}} F(\tilde{\eta})d\tilde{\eta}\right] d\bar{\eta}}{\int_{-\infty}^{\infty} \exp\left[-(S_{O_2}/2)\int_0^{\bar{\eta}} F(\tilde{\eta})d\tilde{\eta}\right] d\bar{\eta}}, \tag{2.4}$$

$$y_{H_2 f} = 1 - \frac{\int_{-\infty}^{\eta} \exp\left[-(S_{H_2}/2)\int_0^{\bar{\eta}} F(\tilde{\eta})d\tilde{\eta}\right] d\bar{\eta}}{\int_{-\infty}^{\infty} \exp\left[-(S_{H_2}/2)\int_0^{\bar{\eta}} F(\tilde{\eta})d\tilde{\eta}\right] d\bar{\eta}}, \tag{2.5}$$

and

$$\frac{\theta_f}{\theta_{-\infty}} = 1 - \frac{\int_{-\infty}^{\eta} \exp\left[-(Pr/2)\int_0^{\bar{\eta}} F(\tilde{\eta})d\tilde{\eta}\right] d\bar{\eta}}{\int_{-\infty}^{\infty} \exp\left[-(Pr/2)\int_0^{\bar{\eta}} F(\tilde{\eta})d\tilde{\eta}\right] d\bar{\eta}}, \tag{2.6}$$

where $\theta_{-\infty} = (T_{-\infty} - T_\infty)/T_\infty$ and where $y_{O_2 f} = Y_{O_2 f}/Y_{O_2 \infty}$ and $y_{H_2 f} = Y_{H_2 f}/Y_{H_2 - \infty}$ are the frozen reactant mass fractions normalized with their corresponding free-stream values. Note that in the simple isovelocity case $u_\infty = u_{-\infty}$, the solution for the stream function reduces to $F = \eta$, while the expressions given in (2.4)–(2.6) simplify to

$$y_{O_2 f} = 1 - \frac{1}{2}\operatorname{erfc}\left(S_{O_2}^{1/2}\eta/2\right), \tag{2.7}$$

$$y_{H_2 f} = \frac{1}{2}\operatorname{erfc}\left(S_{H_2}^{1/2}\eta/2\right), \tag{2.8}$$

and

$$\frac{\theta_f}{\theta_{-\infty}} = \frac{1}{2}\operatorname{erfc}\left(Pr^{1/2}\eta/2\right), \tag{2.9}$$

where erfc is the complementary error function.

Because of the autocatalytic exponential radical growth with distance that will be seen to characterize chain-branching ignition, the effect of reactant consumption is important only close to the ignition point at which the radical mole fractions reach values of order unity corresponding to partial equilibrium of the branching reactions. Hence, reactant consumption can be neglected in the first approximation when determining the ignition distance. This reduces the problem to that of integrating the conservation equations for the chain-branching radicals with the chemical terms evaluated with frozen reactant concentrations and frozen temperature. To write these equations, it is convenient to define normalized H-atom and O-atom mass fractions

$$y_H = \frac{k_{2\infty}}{2k_{1\infty}}\frac{W_{H_2}}{W_H}\frac{Y_H}{Y_{H_2-\infty}} \tag{2.10}$$

and

$$y_O = \frac{k_{2\infty}}{2k_{1\infty}}\frac{W_{H_2}}{W_O}\frac{Y_O}{Y_{H_2-\infty}}, \tag{2.11}$$

together with a new streamwise coordinate

$$\xi = \frac{\rho Y_{O_2\infty} k_{2\infty}}{u_\infty W_{O_2}} x \tag{2.12}$$

scaled with the characteristic air-side branching distance. Here, W_i denotes the molecular weight of species i. In terms of the streamwise coordinate ξ and the similarity coordinate η, required to describe the self-similar profiles of temperature and reactant mass fractions, the radical conservation equations become

$$\frac{\partial y_{\mathrm{H}}}{\partial \xi} - \frac{1}{\xi F'(\eta)}\left(\frac{1}{2}F(\eta)y'_{\mathrm{H}} + \frac{1}{S_{\mathrm{H}}}y''_{\mathrm{H}}\right) = \kappa_{\mathrm{I}}(\eta) + 2\gamma\kappa_{\mathrm{III}}(\eta)\, y_{\mathrm{O}} \tag{2.13}$$

and

$$\frac{\partial y_{\mathrm{O}}}{\partial \xi} - \frac{1}{\xi F'(\eta)}\left(\frac{1}{2}F(\eta)y'_{\mathrm{O}} + \frac{1}{S_{\mathrm{O}}}y''_{\mathrm{O}}\right) = \kappa_{\mathrm{II}}(\eta)\, y_{\mathrm{H}} - \gamma\kappa_{\mathrm{III}}(\eta)\, y_{\mathrm{O}}, \tag{2.14}$$

with boundary conditions $y_{\mathrm{H}} = y_{\mathrm{O}} = 0$ at $\xi = 0$ and at $\eta = \pm\infty$ for $\xi > 0$. Here,

$$\gamma = \frac{k_{3\infty}}{k_{2\infty}}\frac{W_{\mathrm{O}_2}}{W_{\mathrm{H}_2}}\frac{Y_{\mathrm{H}_2-\infty}}{Y_{\mathrm{O}_2\infty}} \tag{2.15}$$

is the ratio of the characteristic branching time of reaction II to that of reaction III, a quantity that depends on the degree of dilution of the fuel stream, becoming very large for undilute fuel feed ($\gamma \simeq 200$). The functions of order unity

$$\kappa_{\mathrm{I}} = \exp[\beta_1\theta_f/(1+\theta_f)]y_{\mathrm{O}_2 f}y_{\mathrm{H}_2 f}/F', \tag{2.16}$$

$$\kappa_{\mathrm{II}} = \exp[\beta_2\theta_f/(1+\theta_f)]y_{\mathrm{O}_2 f}/F', \tag{2.17}$$

and

$$\kappa_{\mathrm{III}} = \exp[\beta_3\theta_f/(1+\theta_f)]y_{\mathrm{H}_2 f}/F', \tag{2.18}$$

where $\beta_j = E_j/(R^oT_\infty)$ is the nondimensional activation energy of the elementary reaction j, represent reduced Damköhler numbers corresponding to reactions I–III evaluated with the local flow velocity and local reactant concentrations at the transverse location η. Note that (2.13) and (2.14) with $F = \eta$ (isovelocity case) and with the time replacing x/u_∞ in the definition of the nondimensional variables η and ξ can also be employed to describe the branching process in the unsteady mixing layer that forms when two half spaces, one of air and the other of hydrogen diluted with nitrogen, are put into contact.

3. Preliminary considerations. The nature of the chemistry of the explosion process can be demonstrated most easily by neglecting diffusion and transverse convection.

3.1. Diffusionless radical growth. With the choice of coordinates in the formulation, the second of the two terms appearing in the brackets on the left-hand side of (2.13) and (2.14) corresponds to radical diffusion, while the first is the apparent transverse convection toward the center of the mixing layer associated with the growth with ξ of the scale used in the definition of η. To help expose the different characteristic regions that appear along the chain-branching mixing layer, it is convenient to remove initially these two terms, thereby precluding transverse transport of radicals. Although this simplifying assumption may appear to hold for the radical evolution at large downstream distances because of the ξ^{-1} factor in these terms in (2.13) and (2.14), more careful study will show that transverse radical diffusion

plays a significant role everywhere along the igniting mixing layer, being in fact the dominant transport mechanism for large ξ. The present approximation therefore is primarily heuristic, designed to explore the general nature of the problem.

Neglecting transverse transport reduces (2.13) and (2.14) to the ordinary differential equations

$$\frac{\partial y_{\mathrm{H}}}{\partial \xi} = \kappa_{\mathrm{I}}(\eta) + 2\gamma\kappa_{\mathrm{III}}(\eta)\, y_{\mathrm{O}} \tag{3.1}$$

and

$$\frac{\partial y_{\mathrm{O}}}{\partial \xi} = \kappa_{\mathrm{II}}(\eta)\, y_{\mathrm{H}} - \gamma\kappa_{\mathrm{III}}(\eta)\, y_{\mathrm{O}}, \tag{3.2}$$

which can be readily integrated with initial conditions $y_{\mathrm{H}}(0) = y_{\mathrm{O}}(0) = 0$ to yield

$$\begin{aligned}\begin{bmatrix} y_{\mathrm{H}} \\ y_{\mathrm{O}} \end{bmatrix} &= \frac{1-\lambda^-/(2\kappa_{\mathrm{II}})}{\lambda^+ - \lambda^-} \begin{bmatrix} \kappa_{\mathrm{I}} \\ \frac{\kappa_{\mathrm{I}}\lambda^+}{2\gamma\kappa_{\mathrm{III}}} \end{bmatrix} \exp(\lambda^+\xi) \\ &\quad - \frac{1-\lambda^+/(2\kappa_{\mathrm{II}})}{\lambda^+ - \lambda^-} \begin{bmatrix} \kappa_{\mathrm{I}} \\ \frac{\kappa_{\mathrm{I}}\lambda^-}{2\gamma\kappa_{\mathrm{III}}} \end{bmatrix} \exp(\lambda^-\xi) - \begin{bmatrix} \frac{\kappa_{\mathrm{I}}}{2\kappa_{\mathrm{II}}} \\ \frac{\kappa_{\mathrm{I}}}{2\gamma\kappa_{\mathrm{III}}} \end{bmatrix},\end{aligned} \tag{3.3}$$

where

$$\lambda^{\pm} = \frac{\gamma\kappa_{\mathrm{III}}}{2}\left(\pm\sqrt{\frac{8\kappa_{\mathrm{II}}}{\gamma\kappa_{\mathrm{III}}} + 1} - 1\right) \tag{3.4}$$

are the roots of the associated characteristic equation

$$\lambda^2 + \gamma\kappa_{\mathrm{III}}\lambda - 2\gamma\kappa_{\mathrm{II}}\kappa_{\mathrm{III}} = 0. \tag{3.5}$$

As can be seen, one of the roots, λ^+, is positive, corresponding to an exponentially growing solution (the first term on the right-hand side of (3.3)), while the other root, λ^-, is negative, giving an exponentially decaying contribution.

3.2. Radical-branching regions. The simplified solution given in (3.3) readily allows us to identify the different regions that emerge in the chain-branching explosion. For convenience, the ratio $\varepsilon = 2k_{1\infty}/k_{2\infty}$ is used as a scale for the radical mass fractions. This quantity, typically extremely small with values at $T_\infty = 1200$ and $T_\infty = 2000$ given approximately by 3.5×10^{-7} and 8.7×10^{-5}, is a measure of the characteristic radical mass fraction for which the rates of the initiation and branching steps are equal. In the early stages of the chain-branching process, i.e., for distances much smaller than the characteristic branching distance ($\xi \ll 1$), the rates of the branching reactions, which are proportional to the concentrations of radicals, are very small, and radical growth depends mainly on the initiation reactions. This initiation-controlled region corresponds to radical mass fractions smaller than the quantity ε and, consequently, to values of y_{H} and y_{O} much smaller than unity. A Taylor expansion of (3.3) in the limit $\xi \ll 1$ yields $y_{\mathrm{H}} = \kappa_{\mathrm{I}}\xi$ and $y_{\mathrm{O}} = \kappa_{\mathrm{I}}\kappa_{\mathrm{II}}\xi^2/2$ for the initial growth of the radicals. As can be observed, since the initiation reaction produces only H atoms, whereas O-atom growth depends exclusively on the branching reaction II, the function y_{O} remains initially smaller than y_{H}.

This initiation-controlled region ends as the radical mass fractions reach small values of order ε, for which the rates of the initiation and branching steps are approximately equal. In the following intermediate region, which corresponds to values of y_{H}, y_{O}, and ξ of order unity, all terms in (3.3) become equally important and must be retained for a correct description of the solution. As ξ further increases to values larger than unity, the exponentially decreasing contribution as well as the particular solution (the third term on the right-hand side of (3.3)) have a negligible effect, so that the solution simplifies to

$$\begin{bmatrix} y_{\mathrm{H}} \\ \\ y_{\mathrm{O}} \end{bmatrix} = \frac{1-\lambda^-/(2\kappa_{\mathrm{II}})}{\lambda^+-\lambda^-} \begin{bmatrix} \kappa_{\mathrm{I}} \\ \\ \frac{\kappa_{\mathrm{I}}\lambda^+}{2\gamma\kappa_{\mathrm{III}}} \end{bmatrix} \exp(\lambda^+\xi), \tag{3.6}$$

yielding radical concentrations growing exponentially with an exponent $\lambda^+(\eta)$ given by (3.4). This exponent corresponds to the local branching Damköhler number associated with the branching steps II and III considered here. Evaluation of λ^+ across the mixing layer reveals that the local branching Damköhler number is maximum at a certain intermediate location across the mixing layer, while $\lambda^+ \to 0$ as $\eta \to \pm\infty$, corresponding to the failure of the branching chemistry in the absence of either one of the two reactants. For sufficiently small values of $u_{-\infty}/u_{\infty}$, not to be considered here, λ^+ will exhibit a second maximum on the low-velocity side of the mixing layer. Equation (3.6) indicates that with transverse transport neglected the radical pool in this region of autocatalytic growth increases at each transverse location as that of a premixed chain-branching explosion, giving a growth rate that is maximum at a certain intermediate transverse location.

In this third region of autocatalytic radical growth the functions y_{H} and y_{O} reach large values, corresponding to radical mass fractions larger than ε, causing the initiation reaction to have a negligibly small rate compared to that of the branching steps, as can be seen from (3.1) and (3.2). Since the values of the radical mass fractions corresponding to partial equilibrium of the branching reactions are typically of order unity, i.e., the values of y_{H} and y_{O} at the ignition point are large quantities of characteristic value ε^{-1}; this third, exponentially growing stage extends over most of the ignition process, taking place over a long distance corresponding to ξ in the range $1 \ll \xi \lesssim \ln[\varepsilon^{-1}]$. Therefore, although transition of the solution from the initiation-controlled region to the region of autocatalytic growth requires consideration of both the exponentially decaying solution and the particular solution arising from the effect of the initiation reactions, most of the ignition history is controlled by the exponentially growing solution. As a consequence, if errors of order unity (small relative errors of order $1/\ln[\varepsilon^{-1}]$) are neglected, then one can calculate the ignition distance ξ_i at each transverse location η by taking logarithms in (3.6) to give in the first approximation

$$\xi_i = \frac{\ln[\varepsilon^{-1}]}{\lambda^+} \tag{3.7}$$

a simplified result that does not require investigation of the short initial period in which the initiation reaction is significant. It is worth remarking that the behavior discussed here in connection with the reduced mechanism I–III can be generalized to more complex chemical systems with a larger number of branching radicals not in steady state. In that case, the order of the corresponding characteristic equation would also be larger (equal to the number of branching radicals not in steady state), and

more than one positive real root, together with negative real roots and even complex roots, may in principle exist, all being important for the description of the initial stages of radical growth. However, as the distance increases sufficiently, the solution corresponding to the maximum positive real root dominates the ignition behavior, so that approximate expressions analogous to (3.6) and (3.7) in general can be found.

3.3. Effect of radical diffusion. Radical diffusion, which was neglected in our introductory analysis, is of fundamental importance to radical growth in mixing layers. Its effect, which will be taken into account below in the description of the initiation-controlled region, is particularly important in the region of autocatalytic growth corresponding to large downstream distances. As previously mentioned, in a naive approach to solving (2.13) and (2.14) in the limit $\xi \gg 1$, it may seem reasonable to discard all the transverse transport terms, which appear multiplied by the small factor ξ^{-1}, yielding, therefore, (3.6) as the solution for the large radical profiles in this region. This simple intuitive description fails, however, in the presence of radical diffusion, as can be seen by substituting the functions given in (3.6) back into (2.13) and (2.14). The diffusion terms, $(\xi S_{\mathrm{H}} F')^{-1} y''_{\mathrm{H}}$ and $(\xi S_{\mathrm{O}} F')^{-1} y''_{\mathrm{O}}$, that were assumed in the preliminary approach to be small, are found to be larger than the terms retained in the analysis by a factor ξ. This finding exposes clearly the predominant role of radical diffusion, which can be easily explained from physical considerations as follows.

With radical diffusion neglected, we have seen that, at each transverse location, radical concentrations grow with distance with an exponential rate proportional to the local effective branching Damköhler number constructed with the local flow velocity, reactant concentration, and temperature. Because of the exponential growth at the location of maximum λ^+, radical concentrations soon become exponentially large compared with radical concentrations elsewhere, thereby leading to the development of sharp peaks in radical profiles. The presence of steep transverse gradients at this location enhances radical diffusion to less populated regions, thus rapidly smoothing the peaks and somewhat uniformizing radical-pool growth across the mixing layer. The extent of this equalizing mechanism and its effect on the resulting ignition distance will be assessed in the following sections by means of a WKB-like asymptotic analysis that employs ξ as an asymptotically large quantity.

4. Radical-growth analysis. With the simplifications introduced, the evolution of the radical mass fractions y_{H} and y_{O} with the downstream distance ξ is given by integration of (2.13) and (2.14) with the aforementioned boundary conditions and with the functions $y_{\mathrm{O}_2 f}$, $y_{\mathrm{H}_2 f}$, and θ_f determined from (2.4)–(2.6). These parabolic equations can be integrated with a simple time-marching method in the coordinate ξ. In particular, for the computations shown below, a Crank–Nicolson procedure was employed in the numerical integrations, with an iterative scheme adopted for the solution of the implicit nonlinear system of equations in η that appear at each ξ. As previously mentioned, three distinct regions emerge as the flow evolves downstream: there is an initiation-controlled regime corresponding to y_{H}, y_{O}, and ξ all being small, an intermediate regime for ξ of order unity where the effects of initiation and branching reactions are equally important, and a region of autocatalytic growth that appears for $\xi \gg 1$. While analysis of the intermediate region requires numerical integration of the conservation equations, both the initiation-controlled region and the region of autocatalytic growth are amenable to analytical solution as shown below.

4.1. Initiation-controlled region ($\xi \ll 1$). For small values of the coordinate ξ, the functions y_{H} and y_{O} admit asymptotic expansions in powers of ξ of the form $y_{\mathrm{H}} =$

$\xi\psi_{H0}+\xi^2\psi_{H1}+\cdots$ and $y_O = \xi^2\psi_{O0}+\xi^3\psi_{O1}+\cdots$, where ψ_{H0}, ψ_{O0}, $\cdots$ are functions of the coordinate η. As previously noted, since the initiation reaction produces only H atoms, while the initial O-atom growth depends exclusively on branching reactions, slow in this region of small radical concentrations, the growth rates of the two branching radicals are initially different. This yields mass fractions increasing with downstream distance according to $y_H \propto \xi$ and $y_O \propto \xi^2$. Substituting the asymptotic expansions for y_H and y_O into (2.13) and (2.14) and collecting terms in powers of ξ yields a set of ordinary differential equations to be solved sequentially for the functions ψ_{H0}, ψ_{O0}, $\cdots$. In particular, the leading-order terms are obtained by integration of

$$\frac{1}{F'}\left[\frac{1}{S_H}\psi''_{H0}+\frac{1}{2}F\psi'_{H0}\right]-\psi_{H0}=-\kappa_I \tag{4.1}$$

and

$$\frac{1}{F'}\left[\frac{1}{S_O}\psi''_{O0}+\frac{1}{2}F\psi'_{O0}\right]-2\psi_{O0}=-\kappa_{II}\psi_{H0}, \tag{4.2}$$

with boundary conditions $\psi_{H0}(\pm\infty) = \psi_{O0}(\pm\infty) = 0$. When the velocity profile is uniform ($F = \eta$), the solution to (4.1) can be written in terms of second-order repeated integrals of the error function [1] $\mathrm{i}^2\mathrm{erfc}$ as

$$\begin{aligned}\psi_{H0} = {} & S_H \mathrm{i}^2\mathrm{erfc}\left[\frac{S_H^{1/2}}{2}\eta\right]\int_{-\infty}^{\eta}\kappa_I\,\mathrm{i}^2\mathrm{erfc}\left[-\frac{S_H^{1/2}}{2}\bar\eta\right]\exp\left(\frac{S_H}{4}\bar\eta^2\right)\,\mathrm{d}\bar\eta \\ & +S_H\mathrm{i}^2\mathrm{erfc}\left[-\frac{S_H^{1/2}}{2}\eta\right]\int_{\eta}^{\infty}\kappa_I\,\mathrm{i}^2\mathrm{erfc}\left[\frac{S_H^{1/2}}{2}\bar\eta\right]\exp\left(\frac{S_H}{4}\bar\eta^2\right)\,\mathrm{d}\bar\eta,\end{aligned} \tag{4.3}$$

with $y_{O_2 f}$, $y_{H_2 f}$, and θ_f evaluated from (2.7)–(2.9). Similarly, once the function ψ_{H0} is computed from the above expression, the solution to (4.2) can be written in terms of fourth-order repeated integrals of the error function [1] $\mathrm{i}^4\mathrm{erfc}$ in the form

$$\begin{aligned}\psi_{O0} = {} & S_O \mathrm{i}^4\mathrm{erfc}\left[\frac{S_O^{1/2}}{2}\eta\right]\int_{-\infty}^{\eta}\kappa_{II}\psi_{H0}\,\mathrm{i}^4\mathrm{erfc}\left[-\frac{S_O^{1/2}}{2}\bar\eta\right]\exp\left(\frac{S_O}{4}\bar\eta^2\right)\,\mathrm{d}\bar\eta \\ & +S_O\mathrm{i}^4\mathrm{erfc}\left[-\frac{S_O^{1/2}}{2}\eta\right]\int_{\eta}^{\infty}\kappa_{II}\psi_{H0}\,\mathrm{i}^4\mathrm{erfc}\left[\frac{S_O^{1/2}}{2}\bar\eta\right]\exp\left(\frac{S_O}{4}\bar\eta^2\right)\,\mathrm{d}\bar\eta.\end{aligned} \tag{4.4}$$

The leading-order asymptotic predictions $y_H = \xi\psi_{H0}$ and $y_O = \xi^2\psi_{O0}$ corresponding to an isovelocity ($F = \eta$) and isothermal ($\theta_{-\infty} = 0$) mixing layer are compared in Figure 4.1 with results of numerical integrations of (2.13) and (2.14). In this computation, as in the rest of the paper, the Schmidt numbers are taken to be $S_{O_2} = 0.74$, $S_{H_2} = 0.19$, $S_O = 0.48$, and $S_H = 0.12$. As can be seen, excellent agreement in H-atom profiles is found even beyond the range of validity of the asymptotic expansions. This unexpected behavior emerges because the effect of branching on the H-atom growth is limited to reaction III, with a rate proportional to y_O. As a result, carrying on the asymptotic analysis to a higher order gives $\psi_{H1} = 0$, i.e., the second nonzero term in the asymptotic expansion for y_H is of order ξ^3, with a coefficient ψ_{H2} that is proportional to ψ_{O0}. This function of order unity achieves somewhat small values, as can be seen in Figure 4.1. Therefore, corrections to $y_H = \xi\psi_{H0}$ are small even for

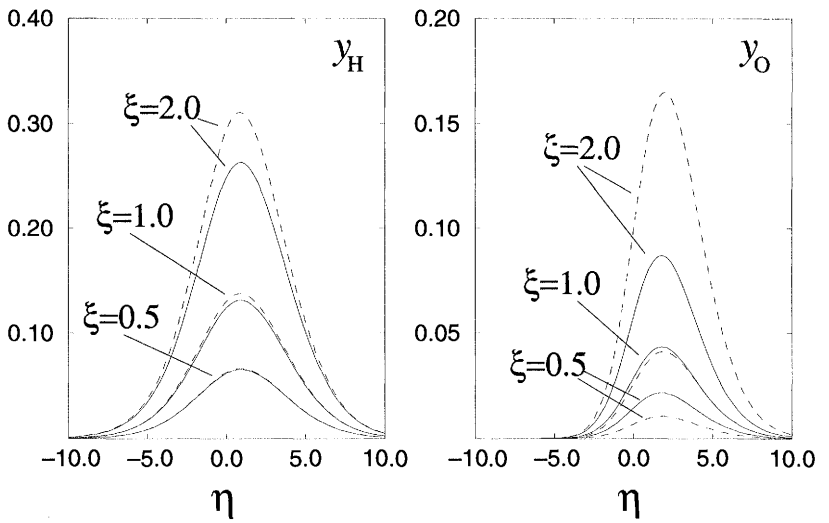

FIG. 4.1. *The functions* y_H *and* y_O *at three different downstream locations along the isovelocity* ($F = \eta$), *isothermal* ($\theta_{-\infty} = 0$) *mixing layer, determined from integrations of* (2.13) *and* (2.14) (*dashed lines*) *and from the leading-order asymptotic predictions* $y_H = \xi\psi_{H0}$ *and* $y_O = \xi^2\psi_{O0}$, *with the functions* ψ_{H0} *and* ψ_{O0} *computed from* (4.3) *and* (4.4) (*solid lines*).

ξ of order unity, thereby extending the range of applicability of this leading-order representation. On the other hand, it can be shown that the next-order term in the expansion for y_O (ψ_{O1}) is nonzero, so that the leading-order expansion $y_O = \xi^2\psi_{O0}$ exhibits inaccuracies of order ξ, as can be seen in Figure 4.1.

4.2. Autocatalytic growth region ($\xi \gg 1$). In this region of exponentially growing radical mass fractions, the initiation term in (2.13) is exponentially small and consequently can be neglected in the analysis that follows. Because of the linearity of (2.13) and (2.14), the solution in the limit $\xi \gg 1$ can be approximated by exponential series of the WKB type [4] of the form

$$y = \exp\left[\xi \sum_{n=0}^{\infty} \xi^{-n/2} G_n(\eta)\right]. \tag{4.5}$$

Since the H-atom and O-atom mass fractions must have the same order of magnitude for the branching chemistry to proceed, one must choose in this approximation the exponentially large terms in the expansions for y_H and y_O to be equal, thereby enabling transport and chemical terms in (2.13) and (2.14) to balance everywhere. Neglecting small terms in the approximated series 4.5 yields

$$\frac{y_H}{\phi_H(\eta)} = \frac{y_O}{\phi_O(\eta)} = \exp[\xi G_0(\eta) + \xi^{1/2} G_1(\eta)], \tag{4.6}$$

where the functions ϕ_H and ϕ_O carry a higher-order η dependence of the solution. Introducing the above expressions into (2.13) and (2.14) and collecting terms of the same order in powers of ξ enables the problem to be solved sequentially as follows.

At leading order (ξ) diffusion dominates, giving the single-term equation

$$G_0'^2 = 0. \tag{4.7}$$

This corresponds to the uniformizing effect of diffusion previously mentioned, indicating that the radical pool grows in the first approximation with uniform exponential rate G_0, which will be determined below by carrying the analysis to a higher order. Since the equation that emerges at the next order ($\xi^{1/2}$),

$$G_0' G_1' = 0, \tag{4.8}$$

is satisfied identically for any constant value of G_0, one needs to investigate the homogeneous linear system of equations

$$\begin{aligned} &\left[G_0 - \frac{G_1'^2}{S_{\mathrm{H}} F'}\right] \phi_{\mathrm{H}} - 2\gamma\kappa_{\mathrm{III}}\phi_{\mathrm{O}} = 0, \\ &-\kappa_{\mathrm{II}}\phi_{\mathrm{H}} + \left[G_0 + \gamma\kappa_{\mathrm{III}} - \frac{G_1'^2}{S_{\mathrm{O}} F'}\right] \phi_{\mathrm{O}} = 0, \end{aligned} \tag{4.9}$$

with boundary conditions $\phi_{\mathrm{H}}(\pm\infty) = \phi_{\mathrm{O}}(\pm\infty) = 0$ that appear at order unity.

Existence of nontrivial solutions to this problem requires that the determinant of the coefficient matrix associated with the above system of equations must vanish everywhere. This condition provides the quadratic equation for $G_1'^2$

$$G_1'^4 - S_{\mathrm{O}} B G_1'^2 + S_{\mathrm{H}} S_{\mathrm{O}} (F')^2 (G_0 - \lambda^+)(G_0 - \lambda^-) = 0, \tag{4.10}$$

where $\lambda^{\pm}$, given above in (3.4), and

$$B = F' \left[\left(\frac{S_{\mathrm{H}}}{S_{\mathrm{O}}} + 1\right) G_0 + \gamma\kappa_{\mathrm{III}}\right] \tag{4.11}$$

are functions of the transverse coordinate η. Equation (4.10) can be easily solved to yield two different solutions:

$$G_1'^2 = S_{\mathrm{O}}(B/2)\{1 \pm [1 - 4(S_{\mathrm{H}}/S_{\mathrm{O}})(F')^2 (G_0 - \lambda^+)(G_0 - \lambda^-)/B^2]^{1/2}\}. \tag{4.12}$$

The solution corresponding to the positive square root never vanishes, thereby giving two G_1 profiles monotonically increasing or decreasing with η. This behavior is not compatible with the boundary conditions $y_{\mathrm{H}} = y_{\mathrm{O}} = 0$ at $\eta = \pm\infty$ and, therefore, these two solutions must be disregarded.

The number of locations where the other solution for $G_1'^2$ vanishes, which are turning points of the WKB expansion [4], depends on the value of G_0, as can be seen from (4.10). For positive values of G_0 corresponding to the exponential autocatalytic growth described here, the turning points are simply the roots of $G_0 = \lambda^+$. Hence, if the value of G_0 is larger than the maximum value that the local Damköhler number λ^+ reaches across the mixing layer, G_0^*, then no turning points appear, and the resulting solutions for G_1 either increase or decrease monotonically with η, which is not acceptable as previously explained. For values of G_0 smaller than G_0^*, the solution would exhibit two turning points, between which the resultant radical profiles would be oscillatory. Since branching chemistry, with rates proportional to radical concentrations, prevents the development of new extrema of radical profiles, the potential appearance of oscillatory behaviors depends upon the initial radical growth history. As can be seen in Figure 4.1, the initiation reaction considered in this case causes the radical profiles to possess a single maximum in the initial stages of the chain-branching explosion, thereby precluding the existence of two turning points across

the mixing layer. Therefore, the asymptotic solution that emerges must exhibit a single turning point, located at the transverse location η^* where λ^+ reaches its peak value, determined from the condition

$$\left[\frac{\mathrm{d}(\lambda^+)}{\mathrm{d}\eta}\right]_{\eta=\eta^*} = 0, \tag{4.13}$$

with λ^+ given in (3.4). Correspondingly, the leading-order exponential growth rate is determined by

$$G_0^* = \lambda^+(\eta^*), \tag{4.14}$$

which is constant across the mixing layer and corresponds to that of the maximum local effective Damköhler number based on the flow velocity. This indicates that radical diffusion does not affect the chain-branching rate in the first approximation. Although this convection-controlled behavior of chain-branching processes in nonpremixed mixing layers was previously pointed out by Treviño and Liñán [14], their conclusion arose from observation of numerical integrations of the conservation equations, rather than from a mathematical analysis such as the one presented here.

Once the values of η^* and G_0^* are obtained as indicated above, one concludes that $G_0 = G_0^*$ and, with G_1^* denoting the value of G_1 at $\eta = \eta^*$, can integrate (4.12) to find

$$G_1 = G_1^* \pm S_{\mathrm{O}}^{1/2} \int_{\eta^*}^{\eta} (B/2)^{1/2}\{1 - [1 - 4(S_{\mathrm{H}}/S_{\mathrm{O}})(F')^2(G_0^* - \lambda^+)(G_0^* - \lambda^-)/B^2]^{1/2}\}^{1/2}\mathrm{d}\eta, \tag{4.15}$$

which gives the asymptotic form of the radical profiles. The boundary conditions at $\eta = \pm\infty$ indicate that one must choose the solution with the positive integral to describe the profiles for $\eta < \eta^*$ and, similarly, the negative integral as $\eta \to \infty$, with transition between both solutions taking place at the turning point, $\eta = \eta^*$, where the radical profiles peak. The maximum value, $G_1^* = G_1(\eta^*)$, of G_1 remains undetermined in the integration. One needs to resolve the structure of the turning point in order to find this value as shown below. Although the explicit determination of the functions ϕ_{H} and ϕ_{O} requires carrying the analysis to the next higher order, solution to the homogeneous system given in (4.9) with $G_0 = G_0^*$ provides the ratio $\phi_{\mathrm{O}}/\phi_{\mathrm{H}}$ across the mixing layer in the form

$$\frac{\phi_{\mathrm{O}}}{\phi_{\mathrm{H}}} = \frac{G_0^* - G_1'^2/(S_{\mathrm{H}}F')}{2\gamma\kappa_{\mathrm{III}}}. \tag{4.16}$$

4.3. Turning-point analysis. The asymptotic solution described by the series in (4.6) holds away from the turning point but breaks down in the vicinity of $\eta = \eta^*$, within a thin layer of characteristic thickness $\xi^{-1/4}$ where second-order spatial derivatives previously neglected in deriving (4.9) have to be retained as can be seen in (4.18) and (4.19) below. In this thin layer, the H-atom and O-atom mass fractions admit descriptions of the form

$$\frac{y_{\mathrm{H}}}{\phi_{\mathrm{H}}^*} = \frac{y_{\mathrm{O}}}{\phi_{\mathrm{O}}^*} = \exp[\xi G_0^* + \xi^{1/2}G_1^*]\ \Psi(\chi), \tag{4.17}$$

where ϕ_{H}^* and ϕ_{O}^* are the unknown values of the functions ϕ_{H} and ϕ_{O} at $\eta = \eta^*$ and $\chi = \xi^{1/4}(\eta - \eta^*)$ is an inner coordinate that has been stretched appropriately. The

function $\Psi(\chi)$ must describe the evolution of the radical profiles across this thin layer from exponentially growing solutions with increasing η for $\eta < \eta^*$, corresponding to the positive branch in (4.15), to the exponentially decaying profiles for $\eta > \eta^*$ (the negative solution in (4.15)), with transition between both branches being possible only for a single value of G_1^*. Introducing the expressions given in (4.17) into (2.13) and (2.14) yields the linear equations

$$\left\{G_0^*\Psi + \xi^{-1/2}\left(\frac{G_1^*}{2}\Psi - \frac{1}{S_{\mathrm{H}}F'}\ddot{\Psi}\right)\right\}\phi_{\mathrm{H}}^* - \{2\gamma\kappa_{\mathrm{III}}\Psi\}\,\phi_{\mathrm{O}}^* = 0 \tag{4.18}$$

and

$$-\{\kappa_{\mathrm{II}}\Psi\}\,\phi_{\mathrm{H}}^* + \left\{(G_0^* + \gamma\kappa_{\mathrm{III}})\,\Psi + \xi^{-1/2}\left(\frac{G_1^*}{2}\Psi - \frac{1}{S_{\mathrm{O}}F'}\ddot{\Psi}\right)\right\}\phi_{\mathrm{O}}^* = 0, \tag{4.19}$$

where $\ddot{\Psi}$ represents the second derivative of the function Ψ with respect to the coordinate χ.

In deriving (4.18) and (4.19), small terms of order $\xi^{-3/4}$ have been neglected. Nontrivial solutions to this problem exist only if the determinant of the coefficient matrix vanishes everywhere. It can be seen that the terms of order unity as well as those of order $\xi^{-1/4}$ that emerge in the resultant characteristic equation vanish automatically following (4.13) and (4.14). The terms emerging at the following order $(\xi^{-1/2})$ yield the parabolic cylinder equation [1]

$$\frac{\partial^2\Psi}{\partial\zeta^2} - \left(\frac{\zeta^2}{4} + \Lambda\right)\Psi = 0, \tag{4.20}$$

where

$$\zeta = [-2S_{\mathrm{H}}(F')^2(\lambda^+)''(\lambda^+ - \lambda^-)/B]^{1/4}\,\chi \tag{4.21}$$

is a renormalized inner coordinate and

$$\Lambda = \left(\frac{S_{\mathrm{H}}C^2}{-2B(\lambda^+)''(\lambda^+ - \lambda^-)}\right)^{1/2}\frac{G_1^*}{2}. \tag{4.22}$$

In these expressions the functions $(F')^2$, $(\lambda^+)''$, $(\lambda^+ - \lambda^-)$, B, and

$$C = (2G_0^* + \gamma\kappa_{\mathrm{III}})F', \tag{4.23}$$

equal to B in the case $S_{\mathrm{H}} = S_{\mathrm{O}}$, are evaluated at $\eta = \eta^*$.

The solution to (4.20) must be nonnegative and decay exponentially to zero as $\zeta \to \pm\infty$ to match with the radical profiles corresponding to the WKB expansion, a behavior that can be achieved only for

$$\Lambda = -1/2, \tag{4.24}$$

giving an associated eigenfunction

$$\Psi = \exp(-\zeta^2/4). \tag{4.25}$$

Equation (4.24), together with the definition of the parameter Λ given in (4.22), determines uniquely the negative value of G_1^* once the location of the turning point

η^* has been obtained from (4.13). It must be noticed that to discriminate the solution $\Lambda = -1/2$ from the discrete set of eigenvalues that satisfy (4.20) with boundary conditions $\psi(\pm\infty) = 0$, one must impose a nonnegativity constraint on the solution. This constraint is associated with the absence of oscillatory radical profiles, a criterion that is also used at leading order to determine the value of G_0^*. Clearly, imposing a nonoscillatory behavior is a key part of the asymptotic solution presented here.

The negative value of G_1^* reflects the influence of radical diffusion on the branching process, causing the maximum radical concentration to increase at a smaller rate, an effect not seen in the leading-order solution that becomes more pronounced for larger radical diffusivities (smaller values of S_H and S_O), as can be seen from (4.22). It can also be observed that, since radical migration from $\eta = \eta^*$ toward the free streams depends on the sharpness of the radical profiles at the radical peaks, the value of G_1^* varies with the curvature of the Damköhler-number distribution at $\eta = \eta^*$ according to $G_1^* \propto [-(\lambda^+)'']^{1/2}$.

5. Discussion of the asymptotic results. To evaluate the utility of the asymptotic analysis it is of interest to explain the characteristics predicted by the asymptotics and to compare the asymptotic results with those of numerical integrations.

5.1. Predictions of radical growth. The asymptotic analysis predicts that at leading order the radical mass fractions are equal to $\exp[\xi G_0^*]$, uniform across the mixing layer, with corrections entering at the following order to yield $\exp[\xi G_0^* + \xi^{1/2} G_1^*]$ for the maximum H-atom and O-atom mass fractions, reached at the turning point location $\eta = \eta^*$. Corrections of order unity, necessary to discriminate between the values of the two branching radicals, would necessitate carrying on the analysis to a higher order to compute the functions ϕ_H and ϕ_O. Since the initiation-controlled region also introduces changes in the resulting solution of order unity, the functions ϕ_H and ϕ_O necessarily contain memory effects associated with the initial region where ξ is of order unity. One can anticipate that the required computation would then involve matching of the asymptotic solution corresponding to $\xi \gg 1$ with the numerical profiles emerging from the intermediate region, resulting in a complicated calculation that is not pursued further here.

The first-order and second-order asymptotic predictions are compared in Figure 5.1 with the peak values of y_H and y_O at each downstream location obtained by numerical integration of (2.13) and (2.14) for the isothermal, $\theta_{-\infty} = 0$, isovelocity mixing layer. Values of γ corresponding to dilute ($\gamma = 5$) and undilute ($\gamma = 200$) fuel feed are considered, for which $\eta^* = 1.82299$, $G_0^* = 1.01493$, and $G_1^* = -1.20261$ and $\eta^* = 3.41359$, $G_0^* = 1.84576$, and $G_1^* = -1.23215$, respectively, as can be obtained from (4.13), (4.14), and (4.22). As can be seen, the effect of radical diffusion on the chain-branching rate, present in the second-order approximation through the negative value of G_1^*, is clearly nonnegligible.

5.2. Ignition distance. An explicit expression for the ignition distance can be calculated from the present results by solving $\exp[\xi_i G_0^* + \xi_i^{1/2} G_1^*] = \varepsilon^{-1}$ to give in the first approximation

$$\xi_i = \frac{\ln(\varepsilon^{-1})}{G_0^*}\left[1 - \frac{1}{\ln(\varepsilon^{-1})^{1/2}}\frac{G_1^*}{(G_0^*)^{1/2}}\right], \tag{5.1}$$

an improved version of (3.7) that accounts for radical diffusion towards the free streams. Note that the above expression gives the value of the large ignition distance with an error of order unity, corresponding to a small relative error of order $1/\ln(\varepsilon^{-1})$.

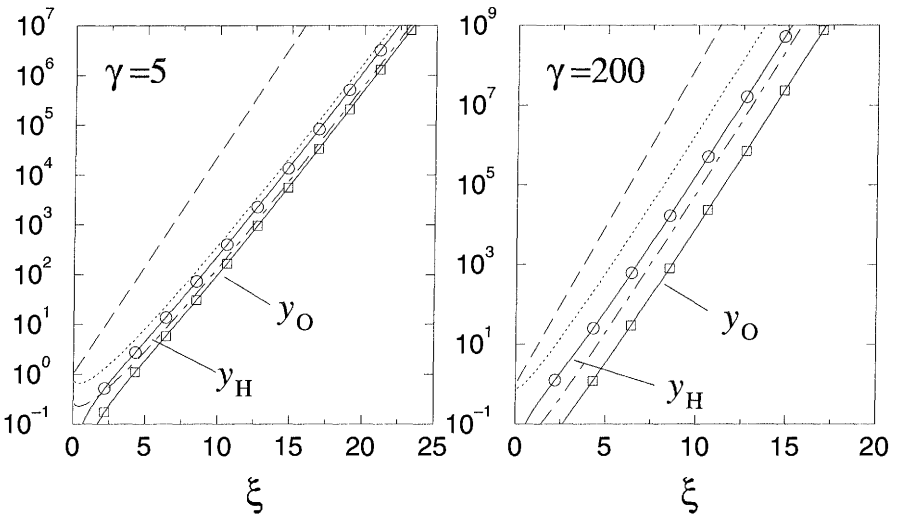

FIG. 5.1. *The evolution with downstream distance of the maximum values of the functions* y_H *(circles) and* y_O *(squares) obtained by integration of* (2.13) *and* (2.14) *for the isothermal* ($\theta_{-\infty} = 0$), *isovelocity* ($F = \eta$) *mixing layer with* $\gamma = 5$ *and* $\gamma = 200$, *and comparison with the leading-order asymptotic prediction* $\exp(G_0^*\xi)$ *(dashed line), the second-order asymptotic prediction* $\exp(G_0^*\xi + G_1^*\xi^{1/2})$ *(dotted line), which apply to both* y_H *and* y_O *at these orders, and O-atom correction* $G_0^* \exp(G_0^*\xi + G_1^*\xi^{1/2})/[2\gamma\kappa_{III}(\eta^*)]$ *(dot-dashed line).*

As previously mentioned, higher accuracy involves carrying on the asymptotic analysis to compute the functions ϕ_H and ϕ_O. Although this analysis is not developed here, the comparisons in Figure 5.1 indicate that (5.1) gives accuracies of ignition distances better than 10%, indicating that the second-order results emerging from the present study are sufficient for practical purposes.

It is of interest to express the ignition distance in the original physical variables. When the effect of radical diffusion is neglected, use of (2.12), (2.15), (2.17), (3.4), and (4.14) in (5.1) yields for the ignition distance x_i

$$x_i = \frac{u^*(1+\sqrt{1+c})\ln[k_{2\infty}/(2k_{1\infty})]}{4\rho k_2^*(Y^*_{O_2 f}/W_{O_2})}, \tag{5.2}$$

where

$$c = \frac{8\kappa^*_{II}}{\gamma\kappa^*_{III}} = \frac{8k_2^* Y^*_{O_2 f}/W_{O_2}}{k_3^* Y^*_{H_2 f}/W_{H_2}} \tag{5.3}$$

is the relevant measure of the ratio of rates of the elementary branching steps 2 and 3. As before, the star ($*$) denotes here the values of the different functions at $\eta = \eta^*$. When the hydrogen stream is undiluted, c is small, and (5.2) becomes

$$x_i = \frac{u^* \ln[k_{2\infty}/(2k_{1\infty})]}{2\rho k_2^*(Y^*_{O_2 f}/W_{O_2})}, \tag{5.4}$$

corresponding to evaluation of (3.7) at the position in the mixing layer where the growth rate of radicals is maximum. In this limit, step 3 is sufficiently rapid that the

growth rate is controlled by the rate of step 2, and in comparison with the order-of-magnitude estimate $x_i = u^*/[\rho k_2^*(Y^*_{O_2 f}/W_{O_2})]$, the present analysis contributes the influence of the initiation step (the logarithmic term) and the factor of two in the denominator. Within the accuracy of the development, the ratio $k_{2\infty}/(2k_{1\infty})$ in the logarithmic term can equally well be replaced by $k_2^*/(2k_1^*)$, the ratio evaluated at the position where the growth rate is maximum, as expected physically. In the opposite limit in which c is large, (5.2) becomes

$$x_i = \frac{u^* \ln[k_{2\infty}/(2k_{1\infty})]}{[2\rho^2 k_2^*(Y^*_{O_2 f}/W_{O_2})k_3^*(Y^*_{H_2 f}/W_{H_2})]^{1/2}}, \tag{5.5}$$

with the effective radical growth rate in the denominator being the geometric mean of the rates of the elementary steps 2 and 3. This occurs because when the effective rate constant for step 2 is large compared with that of step 3, as could be found when the oxidizer stream is pure oxygen and the hydrogen stream is highly diluted, the chemical-kinetic situation is fundamentally different from that of the opposite limit. For small c the O atom achieves steady state, giving a chain-branching step for H equivalent to step I, at a rate proportional to the H-atom concentration [12], but for large c the mechanism of steps I, II, and III do not permit an H-atom steady state. With c large, the rate of the rapid step II is proportional to the H-atom concentration, requiring step III also to occur if step II is to proceed; since the H-atom concentration is proportional to the rate of step III, the effective rate of step II then involves the product of the rate constants for steps 2 and 3, resulting in (5.5).

The first correction to (5.2) for the effect of radical diffusion can be expressed as $x_i = x_i^o(1 + \sqrt{b})$, where x_i^o denotes the value given in (5.2), and

$$b = \frac{[-\kappa_{III}(\sqrt{1 + (8\kappa_{II})/(\gamma\kappa_{III})} - 1)]''^*[(S_H^{-1} + S_O^{-1}) + (S_H^{-1} - S_O^{-1})/\sqrt{1+c}]}{\kappa^*_{III}\{\ln[k_{2\infty}/(2k_{1\infty})]\}F'^*(\sqrt{1+c} - 1)}. \tag{5.6}$$

Here use has been made of (3.4), (4.11), (4.14), and (4.22)–(4.24). The second-derivative factor illustrates the dependence of the diffusion effect on the curvature of the profile at the position of maximum growth rate; for example, in the limit of small c, this factor reduces to $-4\kappa''^*_{II}/\gamma$. The correction $\sqrt{b}$ increases in proportion to the square root of the diffusion coefficients of the radicals and varies inversely with the square root of the local convection velocity, proportional to F'^*. The functional dependences of the increase in the ignition distance caused by tranverse radical diffusion can thus be extracted from the present results.

5.3. Effect of fuel dilution. To investigate the γ dependence of the solution, we plot in Figure 5.2 the variation of G_0^*, G_1^* and η^* with γ in the isovelocity, isothermal mixing layer. As can be seen from (3.4), for very dilute fuel feed ($\gamma \ll 1$) the branching Damköhler number across the mixing layer becomes small according to $\lambda^+ \simeq (2\gamma\kappa_{II}\kappa_{III})^{1/2}$, peaking at an intermediate location given in this case by $\eta^* \simeq 0.875$. The corresponding values of $G_0^* \propto \gamma^{1/2}$ and $G_1^* \propto \gamma^{1/4}$ are also small, indicating that branching is very limited when $\gamma \ll 1$, as could have been anticipated by observing in (2.13) and (2.14) that the growth of H-atoms, which are needed for O-atom branching through the overall step II, is proportional to γ.

A very different behavior is obtained in the case $\gamma \gg 1$, for which the branching Damköhler number given in (3.4) reduces in the first approximation to $\lambda^+ \simeq 2\kappa_{II}$, a function that increases to $\lambda^+ = 2$ as the oxidizer boundary is approached. This simple description corresponds to the assumption of steady state for O, which readily follows

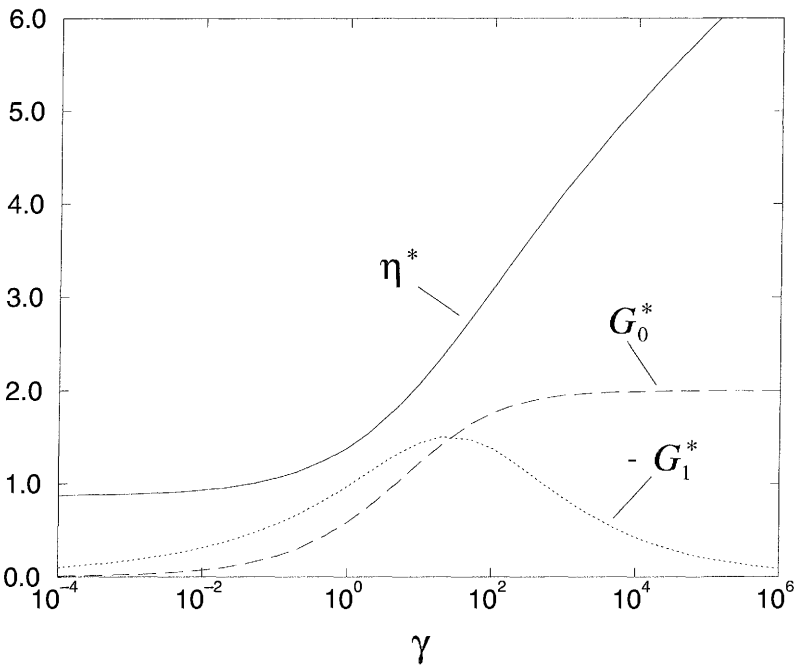

FIG. 5.2. *The variation of* G_0^*, $-G_1^*$ *and* η^* *with* γ *as obtained from* (4.13), (4.14), *and* (4.22) *for the isovelocity* ($F = \eta$), *isothermal* ($\theta_{-\infty} = 0$) *mixing layer.*

from (2.14) in the limit $\gamma \gg 1$, giving small O-atom mass fractions $y_O = \kappa_{II}/(\gamma\kappa_{III})y_H$. This assumption breaks down far on the fuel side, as the H_2 concentration becomes small enough to limit the rate of reaction III, causing λ^+ to decrease eventually to zero for $\eta \to \infty$. Anticipating that at the turning point the value of $\gamma\kappa_{III}$ remains large, one may introduce in (4.13) the approximate expression $\lambda^+ \simeq 2\kappa_{II}[1-2\kappa_{II}(\gamma\kappa_{III})^{-1}]$ corresponding to the first two terms in a Taylor series expansion of (3.4) for $(\gamma\kappa_{III})^{-1} \ll 1$, to yield in the first approximation $\eta^* = [4\ln(\gamma)/(S_{H_2} + S_{O_2})]^{1/2}$ for the isothermal case considered here. Using this estimate in (3.4), one can show that the departures from $\lambda^+ = 2$ at this location are small, of order $\gamma^{-S_{O_2}/(S_{H_2}+S_{O_2})}$. Similarly, one can see that the curvature of the λ^+ profile at $\eta = \eta^*$ is an asymptotically small quantity of order $[\ln(\gamma)]\ \gamma^{-S_{O_2}/(S_{H_2}+S_{O_2})}$. Although radical diffusion is limited by this reduced curvature, causing the value of G_1^* computed from (4.22) to be a small quantity of order $[ln(\gamma)]^{1/2}\ \gamma^{-S_{O_2}/[2(S_{H_2}+S_{O_2})]}$, the effect is partially mitigated because of the large diffusivity of H radicals, an effect that appears through the dependence $G_1^* \propto (S_H)^{-1/2}$. As a result, although G_1^* decreases to zero as $\gamma \to \infty$, it remains of order unity for realistic values of γ corresponding to undilute fuel streams ($\gamma \sim 200$), and radical diffusion therefore must be included for an accurate description of radical growth.

The results presented in Figure 5.1 indicate also that for the two cases considered, both corresponding to large values of γ typical of hydrogen-air combustion, the peak value of y_O remains smaller than that of y_H everywhere, with the difference becoming more pronounced for increasing γ. This behavior can be explained by observing that in the limit $\gamma \to \infty$, the value of ϕ_O at the turning point, assumed in the analysis to be of order unity, becomes smaller than the corresponding value of ϕ_H by a factor $\gamma^{-S_{O_2}/(S_{H_2}+S_{O_2})}$, as can be calculated from (4.16). This ratio could be implemented

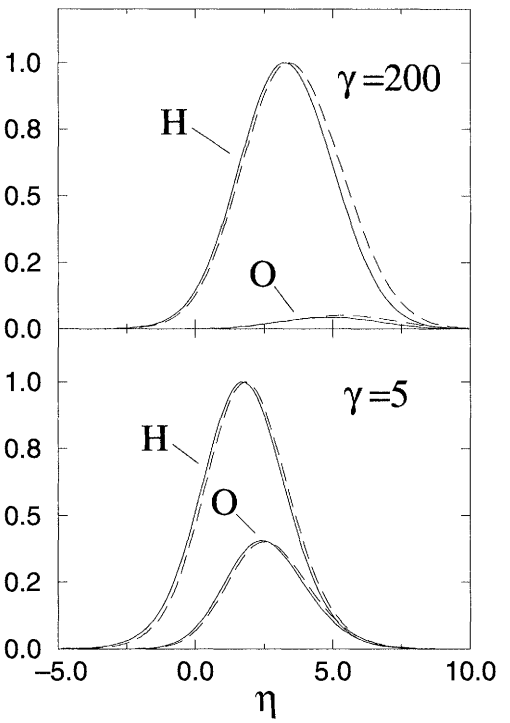

FIG. 5.3. *A comparison for* $\gamma = 5$ ($\xi = 20$) *and* $\gamma = 200$ ($\xi = 15$) *of the radical profiles obtained from integrations of* (2.13) *and* (2.14) *normalized with the maximum H-atom mass fraction* (*solid lines*) *with the asymptotic results* (*dashed lines*) *corresponding to the leading-order representation* $\exp[\xi^{1/2}(G_1(\eta) - G_1^*)]$ *for H atoms and modified representation* $(\phi_O/\phi_H)\exp[\xi^{1/2}(G_1(\eta) - G_1^*)]$ *for O atoms.*

in the analysis to give an improved prediction for O-atom growth, as is done in Figure 5.1, where the dot-dashed curves are obtained by multiplying the second-order prediction of radical peaks, $\exp[\xi_i G_0^* + \xi_i^{1/2} G_1^*]$, by the ratio $\phi_O/\phi_H = G_0^*/[2\gamma\kappa_{III}(\eta^*)]$, determined by evaluating (4.16) at $\eta = \eta^*$.

5.4. The shape of the radical profiles. The shape of the radical profiles appears in the asymptotic analysis at order $\xi^{1/2}$ through the η dependence of G_1 exhibited in (4.15), with corrections of order unity (small relative corrections of order $\xi^{-1/2}$), which are neccesary to differenciate between y_H and y_O, entering at the next order through the functions ϕ_H and ϕ_O. The analysis at order $\xi^{1/2}$ predicts that both radicals peak at $\eta = \eta^*$, yielding profiles, normalized with their maximum values, given in the first approximation by $\exp[\xi^{1/2}(G_1(\eta) - G_1^*)]$, with $G_1(\eta)$ given in (4.15). This representation shows in particular that, although radical diffusion prevents the formation of peaks in radical profiles at leading order, sharp peaks located at $\eta = \eta^*$ appear at order $\xi^{1/2}$, with an inner structure described by (4.25).

Figure 5.1 indicates that in the cases considered ignition is achieved for values of ξ that are only moderately large. Therefore, the small corrections of order $\xi_i^{-1/2}$ that enter the profile shapes through the functions ϕ_H and ϕ_O may be significant at ignition. To investigate further this possible effect, which will be shown to be

important for O atoms, one can evaluate the ratio ϕ_O/ϕ_H given in (4.16) to show that it increases with increasing η, approaching a finite value $\phi_O/\phi_H = [G_0^*(1 - S_H/S_O)]^{-1}$ as $\eta \to \infty$. Because of the higher diffusivity of H-atoms, the O-atom mass fraction decreases on the fuel side much faster than the H-atom mass fraction, with their ratio $\phi_O/\phi_H = \kappa_{II}[G_0^*(1 - S_H/S_O) + \gamma]^{-1} \to 0$ as $\eta \to -\infty$. Therefore, the corrections to the shape of the O-atom profile entering through ϕ_O can be anticipated to be more important than those affecting the H-atom profile, with the effect being enhanced for large values of γ. In particular, the maximum of y_O, which is located at $\eta = \eta^*$ for $\xi \to \infty$, will lie farther into the oxidizer stream for finite values of ξ.

Although the functions ϕ_H and ϕ_O are not computed here, higher-order corrections to the leading-order representation of the radical pool can be incorporated by using (4.16) to modify the O-atom profile, while employing $\exp[\xi^{1/2}(G_1(\eta) - G_1^*)]$ as the representation of the normalized H-atom profile. The results are plotted in Figure 5.3, where the profiles obtained by numerical integration of (2.13) and (2.14) (normalized with the maximum H-atom mass fraction at $\xi = 20$ for $\gamma = 5$ and at $\xi = 15$ for $\gamma = 200$) are compared with the asymptotic predictions $\exp[\xi^{1/2}(G_1(\eta) - G_1^*)]$ for the H-atom profile and $(\phi_O/\phi_H)\exp[\xi^{1/2}(G_1(\eta) - G_1^*)]$ for the O-atom profile. As can be seen, both the shapes and the ratio between the maximum values of y_H and y_O are captured by the analysis. It is also remarkable that memory effects also appear at this finite distances in the H-atom profiles, that are seen to peak to the left of the turning point, as corresponds to a solution that evolves from the initiation-controlled profiles shown in Figure 4.1. These memory effects are, however, not extremely large at the values of ξ in Figure 5.3.

6. Conclusions. This study has shown that histories of the development of branched-chain explosions in high-temperature mixing layers can be described well by asymptotic methods. As the initially nonpremixed reactants flow downstream from a splitter plate and interdiffuse, several different regions can be identified. There is a short chain-initiation region in which chain-carrying radicals are formed from the initial reactants, followed by a long autocatalytic chain-branching region in which chain-carrier concentrations increase exponentially with downstream distance, then a short region in which radical-radical interaction cause the chain carriers to rapidly attain partial equilibrium, with nearly constant mass fractions of order unity, prior to onset of significant exothermicity. The ignition distance is controlled mainly by the long region of autocatalytic radical growth.

Asymptotic expansions about the initial state and also for the long-time development of the autocatalytic growth demostrate that diffusion, convection, and finite-rate chemistry all remain important throughout the explosion history, with diffusive loss of radicals becoming increasingly predominant as the ignition point is approached. The regular expansions for the initiation period are expressible in terms of integrals of error functions, while methods of the WKB type are needed to describe the asymptotic behavior in the autocatalytic region. In the latter approach, a turning point of the second order occurs at the transverse location where the chain-carrier concentrations are maximum. Although the analysis is given only for hydrogen-oxygen mixing layers in which H and O atoms are the only intermediate chemical species not satisfying a chemical-kinetic steady state, the methods clearly can be generalized to account for any number of independent chain carriers and branching steps, resulting in the same type of reactive mixing-layer structure just prior to ignition. Although the parabolic partial differential equations that describe these explosions in mixing layers can now readily be handled by numerical integration, the asymptotic methods are helpful for

providing scaling and formulas that yield parametric dependences of reaction-region structures, chain-carrier evolution and ignition distances.

It is worth mentioning that a variant of the method developed here was recently applied in [12] to study the hydrogen-oxygen chain-branching process in the mixing layer when ignition occurs in the wake that appears associated to the boundary layers of the merging streams. The analysis, which required only consideration of a single radical not in steady state, was carried to a higher order, revealing that the third term in the asymptotic expansion for the radical mass fraction is a switchback logarithmic term, which is also expected to emerge in the present analysis, thereby slightly modifying the expression for the asymptotic expansion given in (4.5). Since it was found [12] that this logarithmic term does not depend on the transverse coordinate η, we can conclude that this higher-order correction would not modify the shape of the radical profiles shown in Figure 5.3, its effect entering only as a relatively small correction in the prediction for the peak radical mass fractions, which can be anticipated to be of the form $\exp[G_0^*\xi + G_1^*\xi^{1/2} + G_2^* \ln(\xi)]$. Although the value of G_2^* was not determined above, the two-term expansion $\exp[G_0^*\xi + G_1^*\xi^{1/2}]$ calculated here clearly suffices to provide sufficient accuracy in the cases covered by the present analysis, as can be seen in Figure 5.1.

REFERENCES

[1] M. Abramowitz and A. Stegun, *Handbook of Mathematical Functions*, Dover, New York, 1965.

[2] G. Balakrishnan, M. D. Smooke, and F. A. Williams, *A numerical investigation of extinction and ignition limits in laminar nonpremixed counterflowing hydrogen-air streams for both elementary and reduced chemistry*, Combust. Flame, 102 (1995), pp. 329–340.

[3] G. Balakrishnan and F. A. Williams, *Turbulent combustion regimes for hypersonic propulsion employing hydrogen-air diffusion flames*, J. Propulsion Power, 10 (1994), pp. 434–436.

[4] C. M. Bender and S. Orszag, *Advanced Mathematical Methods for Scientists and Engineers*, McGraw–Hill, New York, 1978.

[5] A. Liñán, *The asymptotic structure of counterflow diffusion flames for large activation energies*, Acta Astronautica, 1 (1974), pp. 1007–1039.

[6] A. Liñán and A. Crespo, *An asymptotic analysis of unsteady diffusion flames for large activation energies*, Combust. Sci. Tech., 14 (1976), pp. 95–117.

[7] A. L. Sánchez, A. Liñán, and F. A. Williams, *A bifurcation analysis of high-temperature ignition of H_2-O_2 diffusion flames*, in 25th Symposium (International) on Combustion, The Combustion Institute, Pittsburgh, 1994, pp. 1529–1537.

[8] A. L. Sánchez, G. Balakrishnan, A. Liñán, and F. A. Williams, *Relationships between bifurcation and numerical analyses for ignition of hydrogen-air diffusion flames*, Combust. Flame, 105 (1996), pp. 569–590.

[9] A. L. Sánchez, *Nonpremixed spontaneous ignition in the laminar wake of a splitter plate*, Phys. Fluids, 9 (1997), pp. 2032–2044.

[10] A. L. Sánchez, A. Liñán, and F. A. Williams, *A WKB analysis of radical growth in the hydrogen-air mixing layer*, J. Engrg. Math., 31 (1997), pp. 119–130.

[11] A. L. Sánchez, A. Liñán, and F. A. Williams, *A generalized Burke-Schumann formulation for hydrogen-oxygen diffusion flames maintaining partial equilibrium of the shuffle reactions*, Combust. Sci. Tech., 123 (1997), pp. 317–345.

[12] A. L. Sánchez, I. Iglesias, and A. Liñán, *An asymptotic analysis of chain-branching ignition in the laminar wake of a splitter plate separating streams of hydrogen and oxygen*, Combust. Theory Model., 2 (1998), pp. 259–271.

[13] C. Treviño, *Ignition phenomena in H_2-O_2 mixtures*, Progress in Astronautics and Aeronautics, AIAA, 131 (1991), pp. 19–43.

[14] C. Treviño and A. Liñán, *Mixing layer ignition of hydrogen*, Combust. Flame, 103 (1995), pp. 129–141.

[15] F. A. Williams, *Combustion Theory*, Benjamin Cummings, Menlo Park, CA, 1985.